THE INSTITUTE FOR SYSTEMS RESEARCH

ISR TECHNICAL REPORT 2008-21

Multiscale Simulation of Atomic Layer Deposition in a Nanoporous Material

Dwivedi, Vivek, and Adomaitis, Raymond

Multiscale simulation of atomic layer deposition in a nanoporous material

Vivek Dwivedi and Raymond A. Adomaitis
Department of Chemical and Biomolecular Engineering and Institute for Systems Research, University of Maryland, College Park, MD, 20742, adomaiti@umd.edu

Abstract

A multiscale simulator for alumina film growth inside a nanoporous material during an atomic layer deposition process is developed. The model combines a continuum description at the macroscopic level of precursor gas transport inside a nanopore during exposure to each of the two precursor species (trimethyaluminum and water) with a lattice Monte Carlo simulation of the film growth on the microscopic scale. Simulation results are presented for both the Monte Carlo simulation and for the multiscale system, the latter illustrating how nonuniform deposition along the nanopore can occur when insufficient precursor exposure levels are used.

1 Simulation of film growth in ALD

Atomic Layer Deposition (ALD) is a thin film deposition process in which the growth surface is exposed to reactive precursor gases in an alternating fashion. A characteristic of the surface adsorption and reaction mechanisms is that they are normally self limiting, allowing for atomically accurate control of film thickness and uniform deposition over complex surface topologies.

ALD is an important unit operation in manufacturing nanoscale devices. ALD, in fact, is the key enabling technology in Intel's current 45nm transistor technology where it is used to deposit the HfO_2 gate oxide [2]. Another example of ALD use is the production of the nanolaminates for large-scale flat-panel electroluminescence displays [11]. ALD has even greater potential in future manufacturing and research applications, such as in the deposition of gate dielectrics for carbon nanotube transitors [12], nanoelectrodes for studying single molecules [9], and other nanoparticle [10] and nanolaminate [6] applications.

ALD is an inherently dynamic process characterized by multiple time scales: a faster time scale corresponding to the molecular events taking place during each exposure cycle, and the slower *overall* nucleation and steady growth[1] time scales [8]. Likewise, multiple length scales are found in these systems where macroscopic length scales (100's of μm) correspond to gas phase transport effects, and microscopic scales characterize the atomistic nature of the film growth. An approach to coupling modeling elements across these scales to simulate ALD growth of alumina films inside nanopores of high aspect ratio is the topic of this letter.

1.1 Al_2O_3 ALD

We consider Al_2O_3 ALD, one of the most widely studied ALD systems (see, e.g., [3, 14]) and the material system used to modify nanostructured catalytic membrane pore size [5, 13]. Amorphous Al_2O_3

[1] The cycle-integrated growth rate defining the total film thickness added during each exposure cycle.

$P_A =$

↓ from / to →	1	2	3	4
3	1	0	0	0
4	1	0	0	0
6	0	1	0	0
8	0	0	0.5	0.5

$P_W =$

↓ from / to →	2	5	6	7	8
1	1	0	0	0	0
2	0	0	0	1	0
4	0	0	1	0	0
5	0	0.9	0.1	0	0
7	0	0	0	0	1

Table 1: *Transition probability arrays states during TMA (P_A) and water (P_W) exposures.*

films can be grown from alternate exposures of the growth surface to TMA ($Al(CH_3)_3$) and water. To simulate film growth using a lattice Monte Carlo (MC) method, we first discretize the growth surface into a lattice, with lattice element size determined by the minimum number of surface groups necessary to allow for the correct film stoichiometry (Fig. 1) and experimentally measured growth-per-cycle (GPC) rates of typically 1.1Å per ALD processing cycle.

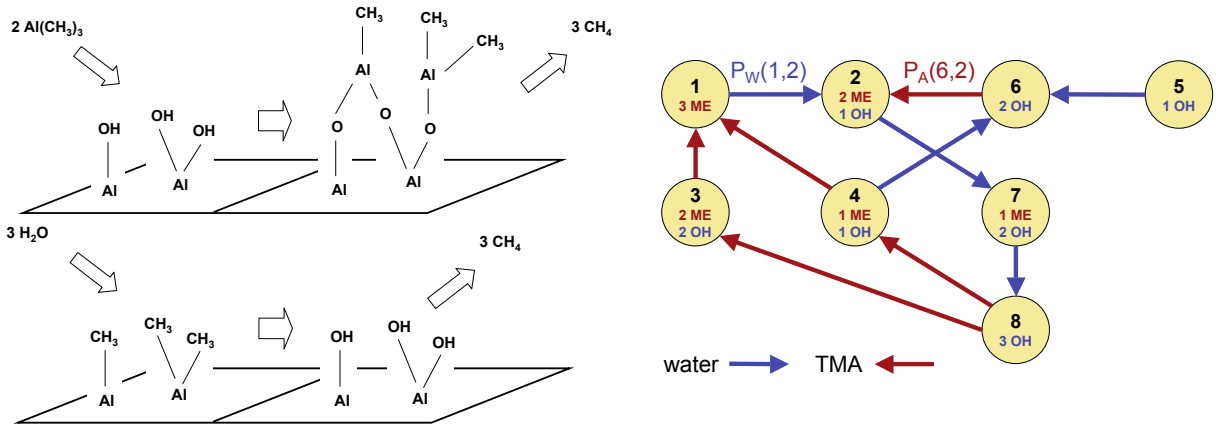

Figure 1: *Ideal Al_2O_3 ALD, after [3], showing the reactions resulting from exposure to TMA (left top) and then to water (left bottom); lattice states 1-8 and a graph of the potential transitions between states (right) during TMA (red arows) and water (blue) exposures; ME denotes CH_3 surface groups.*

Represented in Fig. 1 (left) are the reactions that take place under ideal ALD conditions during exposure of the growth surface to sufficient dosages of TMA and then to water. In reality, exposure of the growth surface to each of the precursors does not guarantee complete conversion of the surface groups and this simple picture cannot describe nucleation, therefore, a more accurate picture of the configuration of each lattice site is obtained by enumerating all possible lattice states (Fig. 1, right). The probability that a lattice site changes from one state to another when a TMA or water precursor molecule interacts with that site is quantified by the transition probabilities associated with the edges of this directed graph. We see that this graph-based framework for understanding the ALD process gives insight into the details of what takes place in the idealized view of ALD presented in Fig 1, showing the different paths one can take from state 1 (all CH_3 surface groups) to state 8 (fully hydroxylated surface) and back again. Notice, also, that stoichiometry is preserved regardless of the cycle taken in this graph. Transition probabilities associated with each edge of the graph are given in Table 1, where for each transition array, the diagonal elements are $P(i,i) = 1 - \sum_{j=1, j\neq i}^{8} P(i,j)$. A more detailed discussion of this surface reaction model is provided in [4].

1.2 The MC algorithm

As stated previously, the ALD process is inherently dynamic, with the growth surface exposed to a time dependent precursor partial-pressure profile that depends on gas-phase transport and surface reactions on the scale of the overall deposition system. In our simulation approach, we focus on a microscopic region of the growth surface and discretize this region into an $N \times N$ grid of lattice sites, stored as an array X. During each exposure cycle, we consider a total of M_i possible transition events, where $M_i = aZ(T)\delta_i\tau_i N^2$ where δ_i is a mean partial pressure of the precursor $i = A, W$ during the exposure cycle, τ_i is the period over which the growth surface is exposed, $Z(T)$ is the temperature-dependent wall collision frequency of the gas per unit area, and a is a constant. This means we fix the number of MC iteration steps during each exposure, rather than the overall time of the half cycle (as would be done in a kinetic MC approach [7]).

During each half reaction period ($i = A, W$), $m = 1, \ldots, M_i$ Monte Carlo iterations are performed in which a lattice site is randomly chosen and the state of that site $\sigma = X_{j,k}$ is determined. The state is used to identify the appropriate row in transition probability array P_i, and a second random number is generated (uniformly distributed in the unit interval) and is compared to the cumulative sum of row σ of P_i, determining which transition (if any) takes place. A full exposure cycle consists of M_A iterations corresponding to the TMA precursor exposure, and M_W iterations for water.

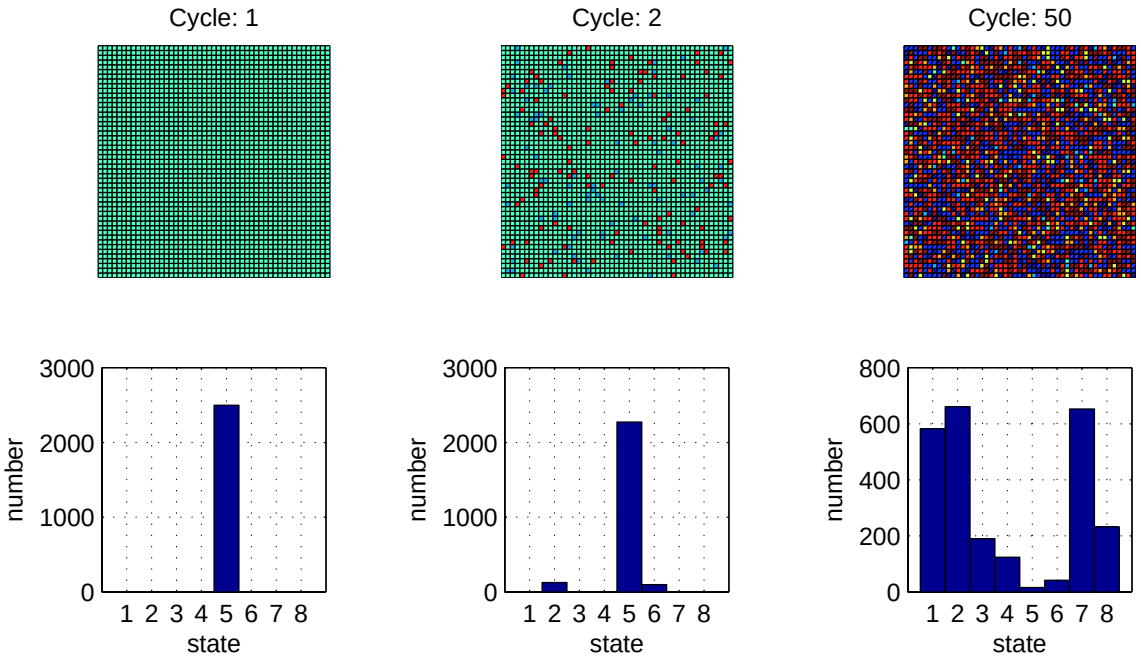

Figure 2: *Representative results of the MC algorithm showing the states of the growth surface lattice after 1, 2, and 50 cycles (from the left) and the corresponding surface state distributions.*

1.3 Results

Representative results of our microscopic simulator are shown in the form of surface region snapshots in Fig. 2. In this figure, we see that the initial condition of the growth surface is the hydroxilated native

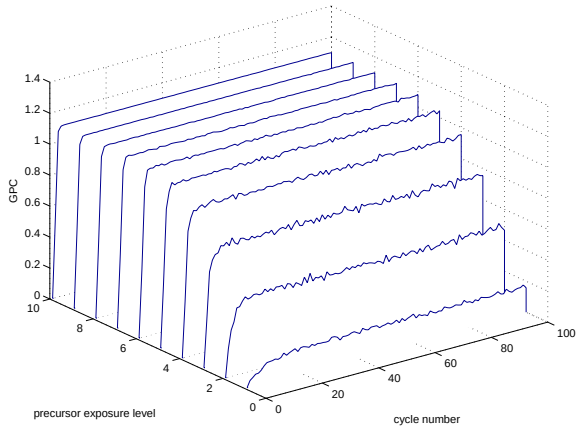

Figure 3: *Overall film growth (growth per cycle, GPC, in Å) versus cycle number for a range of precursor exposure levels δ_A illustrating the nucleation and steady growth phases as well as the self-limiting nature of ALD at sufficiently high precursor exposure levels.*

oxide surface of a silicon wafer (state 5 of Fig. 1), and after one exposure cycle (cycle 2), little has changed. This corresponds to the nucleation stage of film growth; subsequent cycles (e.g., cycle 50), show a much wider range of surface states during this ALD process.

The mean incorporation rate of aluminum can be used to determine the growth rate after each cycle; plotting the dynamics of film growth in terms of GPC (Å of growth per cycle), we see by Fig. 3 the distinct nucleation phase followed by steady film growth. One of the key features of ALD – that the growth becomes self-limited when the surface is not starved for precursors – is seen in this figure. Ideal ALD growth is found for precursor exposure levels of $\delta_A = 6$ or more. We note that $\delta_W = 3\delta_A/2$ in this simulation.

2 Multiscale simulation

To simulate a complete ALD process in a real physical system, we combine the microscopic scale film growth simulator with significantly longer length scale descriptions of gas phase transport and film thickness profiles along the length of a $250\mu m$ nanopore (Fig. 4). Consider a highly simplified description of gas phase transport and surface reaction of the TMA precursor in a nanopore, where gas phase transport is described by Knudsen diffusion[2]:

$$\frac{\partial p_A}{\partial t} = \frac{\partial}{\partial s} D_A \pi R^2(s) \frac{\partial p_A}{\partial s} - \pi R(s) C_A(p_A) \tag{1}$$

where $p_A(s,t)$ is the partial pressure of TMA inside the nanopore, $R(s)$ is the local pore radius, $0 \leq s \leq 1$ is the dimensionless axial coordinate of the pore, and C_A is the local consumption rate of the TMA precursor by the surface reaction. A similar modeling equation exists for the water partial pressure. Because ALD is a cyclic process, one simplification we use is to average (1) over the TMA exposure (half) cycle, giving a *local precursor dosage* δ_A for the TMA precursor (δ_W for water) as a function of spatial position along the pore:

$$\delta_A(s) = \int_0^{\tau_A} p_A(s,t)dt, \qquad c_A(\delta_A(s)) = \int_0^{\tau_A} C_A(p_A(s,t))dt.$$

[2]See the work on tungsten CVD in a trench by Cale and co-workers, e.g., [15] for justification of this modeling approach.

The resulting boundary value problem, subject to a specified exposure level at each end of the pore ($s = 0, 1$) is given by:

$$\frac{d}{ds} D_A R^2(s) \frac{d\delta_A}{ds} - R(s) c_A(\delta_A) = 0 \quad \text{subject to} \quad \delta_A(0) = \delta_A(1) = \delta_A^o.$$

The boundary value problems are discretized using orthogonal collocation [1]; note that the dose-averaged rate terms c_A must be evaluated at each collocation point using the lattice Monte Carlo simulators, resulting in a numerical problem combining a pore-scale continuum description of transport in the nanopore and a sequence of microscopic simulator elements (Fig. 4) for film growth.

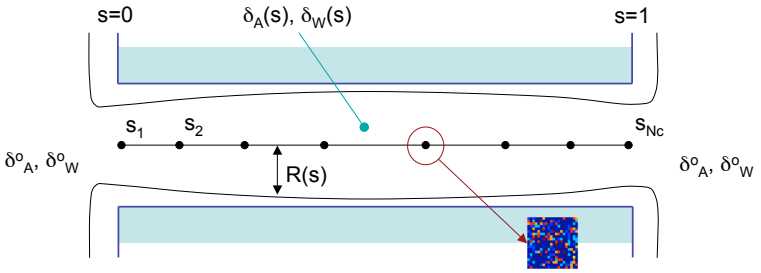

Figure 4: *Pore geometry illustrating the macroscopic scale s over which which the cycle-averaged TMA and water partial pressures (δ_A and δ_W, respectively) are defined. Individual MC models are evaluated at the collocation points s_n.*

The macroscopic variables for the system are the half-cycle averaged precursor partial pressures $\delta_A(s)$ and $\delta_W(s)$, and because of the stochastic nature of the microscopic models that are used to determine c_A and c_W, the spatially discretized modeling equations cannot be written explicitly. Instead, the current solution profile estimates $\delta_A(s)$ and $\delta_W(s)$ are used to determine the number of MC simulation steps in a sequence of microscopic simulations, each located at one of the collocation points, determining the local reactant consumption rate $c_A(s_n)$ and $c_W(s_n)$. The residuals of the modeling equations thus are determined; during each microscopic simulation, we also compute the sensitivity of each $c_A(s_n)$ and $c_W(s_n)$ to $\delta_A(s_n)$ and $\delta_W(s_n)$, respectively. These sensitivities, along with the collocation discretization arrays for the differential terms in the macroscopic modeling equations, define the elements of the Jacobian array needed for the Newton-Raphson procedure used to iteratively solve the macroscopic modeling equations.

The entire numerical approach is implemented using object-oriented elements of MATLAB, and representative results are shown in Fig. 5. In this simulation, the nanopore initially has a uniform radius of 100Å and the boundary condition precursor exposure levels are chosen as $\delta_A^o = 2$ and $\delta_W^o = 3$, levels that normally result in slight starvation of the growth surface. The TMA and water precursors diffuse into the open ends of the nanopore during each exposure step, and a portion is adsorbed onto the pore walls. Early in the deposition process (e.g., after cycle 2), we observe only a small amount of precursor depletion in the innermost regions of the pore. However, the depletion effects grow with increasing number of deposition cycles, leading to preferential deposition near the pore mouths, further accelerating the development of the cycle-averaged precursor partial pressure $\delta_A(s)$ gradients. The simulations were performed for a total of 170 ALD cycles, after which the pore mouths essentially close, preventing further deposition within the pore. This example illustrates the potential for our numerical methods to capture the correct reaction and transport phenomena of the ALD process.

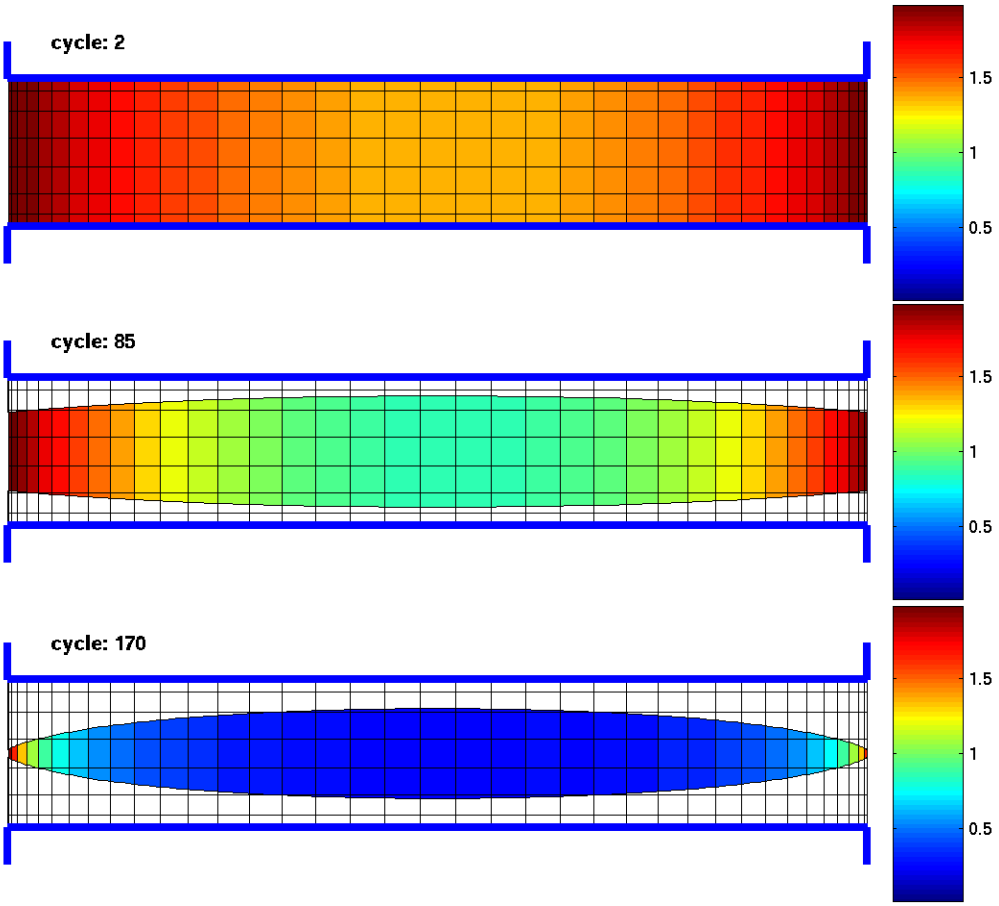

Figure 5: *Deposited pore film thickness is shown in white, original pore outline in blue, along with the gas phase TMA time-averaged partial pressure. Profiles correspond to cycle 2 (top), 85 (middle), and 170 (bottom), where near pore closure occurs in the last.* $\delta_A^o = 2$ *and* $\delta_W^o = 3$ *in this simulation.*

3 Conclusions

A multiscale simulator for the atomic layer deposition of alumina inside a nanoporous material was presented that incorporated two major numerical ideas novel to our approach:

- The spatially distributed and time-dependent problem was simplified by considering the half-cycle averaged equations; this also simplified the microscopic simulations because kinetic (dynamic) Monte Carlo simulations were not required;
- Because the spatially distributed microscopic simulators are not correlated, the sensitivity of each microscopic model's prediction of local precursor consumption rate depends only on local, cycle-averaged precursor exposure levels. This observation greatly simplifies construction of the Jacobian array because the off-diagonal elements correspond only to macroscopic-scale modeling terms (the collocation discretiztion arrays).

Combined, these two important numerical simplifications results in a computationally efficient simulator, useful for exploring factors that give rise to nonuniformities in pore size modification by ALD processes. A more systematic study of simulator predictions is underway.

Acknowledgments

The authors acknowledges the support of the National Science Foundation through grant CTS-0554045.

References

[1] Adomaitis, R. A., Objects for MWR, *Computers & Chem. Engng* **26** (2002) 981-998.

[2] Bohr, M. T. R. S. Chau, T. Ghani, and K. Mistry, The high-k solution, *IEEE Spectrum* Oct. 2007.

[3] Dillon, A. C., A. W. Ott, J. D. Way, and S. M. George, Surface chemistry of Al_2O_3 using $Al(CH_3)_3$ and H_2O in a binary reaction sequence, *Surf. Sci* **322** (1995) 230-242.

[4] Dwivedi, V. and R. A. Adomaitis, Lattice Monte Carlo simulation of amorphous alumina growth during atomic layer deposition, *manuscript in preparation* (2008).

[5] Elam, J. W., G. Xiong, C. Y. Han, H. H. Wang, J. P. Birrell, U. Welp, J. N. Hryn, M. J. Pellin, T. F. Baumann, J. F. Poco, and J. H. Satcher, Jr., Atomic layer deposition for the conformal coating of nanoporous materials, *J. Nanomaterials* (2006) 1-5.

[6] Elam, J. M., Z. A. Sechrist and S. M. George, ZnO/Al_2O_3 nanolaminates fabricated by atomic layer deposition: growth and surface roughness measurements, *Thin Solid Films* **414** 43-55 (2002).

[7] Fichthorn, K. A. and W. H. Weinberg, Theoretical foundation of dynamic Monte Carlo simulations, *J. Chem. Phys.* **95** (1991) 1090.

[8] Granneman, E., P. Fischer, D. Pierreux, H. Terhorst, P. Zagwijn, Batch ALD: Characteristics, comparison with single wafer ALD, and examples, *Surf. Coatings Tech.* **201** 8899-8907 (2007).

[9] Gupta, R. and B. G. Willis, Nanometer spaced electrodes using selective area atomic layer deposition, *Appl. Phys. Lett.* **90** (2007) 253102.

[10] King, D. M., J. A. Spencer II, X. liang, L. F. Hakim, and A. W. Weimer, Atomic layer deposition on particles using a fluidized bed reactor with in situ mass spectrometry, *Surf. Coatings Tech.* **201** 9163-9171 (2007).

[11] A history of electroluminescent displays

`http://www.indiana.edu/~hightech/fpd/papers/ELDs.html`

[12] Javey, A. H. Kim, M. Brink, Q. Wang, A. Ural, J. Guo, P. McINtyre, P. McEuen, M. Lundstrom, and H. Dai, High-k dielectrics for advanced carbon-nanopore transistors and logic gates, *Nature Mater.* **1** 241-246 (2002).

[13] Pellin, M. J., P. C. Stair, G. Xiong, J. W. Elam, J. Birrell, L. Curtiss, S. M. George, C. Y. Han, L. Iton, H.Kung, M. Kung, and H.-H. Wang, Mesoporous catalytic membranes: Synthetic control of pore size and wall composition *Cat. Lett.* **102** (2005) 127-130.

[14] Puurunen, R. L., Surface chemistry of atomic later deposition: A case study of the trimethylaluminum/water system, *Appl. Phys. Rev.* **97** 121301 (2005).

[15] Song, L., S. Shen, K. S. Tsakalis, P. E. Crouch, and T. S. Cale, Optimal control for increasing throughput in low pressure chemical vapor deposition, *Proc. 35th CDC*, Dec. 1996.